PERGAMON

Acta mater. 48 (2000) 3261–3269

Acta MATERIALIA

www.elsevier.com/locate/actamat

TENSILE TESTING OF FREE-STANDING Cu, Ag AND Al THIN FILMS AND Ag/Cu MULTILAYERS

HAIBO HUANG† and F. SPAEPEN‡

Division of Engineering and Applied Sciences, Harvard University, Cambridge, MA 02138, USA

(Received 8 October 1999; accepted 27 February 2000)

Abstract—Free standing polycrystalline thin films with a strong ⟨111⟩ texture were tested in uniaxial tension. Studied were electron-beam deposited Ag, Cu and Al films, and Ag/Cu multilayers consisting of alternating Ag and Cu layers of equal thickness, between 1.5 nm and 1.5 μm (bilayer repeat length, λ, between 3 nm and 3 μm). The films had a total thickness of about 3 μm. A thin polymeric two-dimensional diffraction grid was deposited on the film surface by microlithographic techniques. Strains were measured *in situ* from the relative displacements of two laser spots diffracted from the grid. The average values of the Young's moduli, determined from hundreds of measurements, are 63 GPa for Ag, 102 GPa for Cu, 57 GPa for Al and 87.5 GPa for Ag/Cu multilayers. In all cases, these values are about 20% lower than those calculated from the literature data and, for the Ag/Cu multilayers, are independent of λ. No "supermodulus" effect was observed. The 20% reduction in modulus is most likely the result of incomplete cohesion ("microcracking") of the grain boundaries. The ductility of the Ag/Cu multilayers decreases when λ is reduced. For $\lambda < 80$ nm, the films are brittle at room temperature: they break without macroscopic plastic flow. For $\lambda > 80$ nm, the yield stress increases with decreasing λ according to a Hall–Petch-type relation. No softening with decreasing grain size was observed even at the lowest values of λ. © *2000 Acta Metallurgica Inc. Published by Elsevier Science Ltd. All rights reserved.*

Keywords: Metals; Thin films; Stress–strain relationship measurements; Mechanical properties (elastic); Mechanical properties (yield phenomena)

1. INTRODUCTION

Thin films are particularly well-suited for the systematic study of a central problem in materials science: the relation between the length scales of the microstructure and the physical properties [1]. Adjustment of the deposition conditions and film thickness makes it possible to vary the grain size systematically. Well-controlled deposition of alternating layers of different composition produces a composition modulation and grain sizes on the order of the layer thickness.

Mechanical properties are particularly sensitive to the microstructural length scale. This is even the case for elastic deformation: although earlier claims of greatly enhanced moduli arising from a small-scale composition modulation [2, 3] have by now been laid to rest [4, 5], thin films often appear to be more compliant than their bulk equivalents [6, 7], presumably for microstructural reasons such as imperfectly formed grain boundaries. The increase of the yield stress with decreasing grain size has been known for years and is customarily expressed by an inverse power law, known as the Hall–Petch relation [8–10]. The validity and importance of the Hall–Petch relation (in particular the "classical" exponent of −0.5) are still under debate, both experimentally and theoretically. This is particularly the case if the grains are very small, as in nanocrystalline compacts or multilayered thin films. On theoretical grounds, one expects a transition from a pile-up-type mechanism to a single dislocation mechanism [11], or from dislocation cutting to bowing of dislocations with a decreased line tension [12]. In some cases, even *softening* with decreasing grain size has been observed [13, 14]. These questions are addressed in this work by tensile testing of free-standing homogeneous thin films of three metals (Cu, Ag and Al) and a series of multilayered Ag/Cu thin films, in which the repeat length, and hence the grain size, is systematically varied.

The mechanical properties of thin films are often tested on a substrate, for example by radius-of-curvature measurements during thermal cycling [15] or nano-indentation [14]. The constraint provided by

† Present address: Corning Inc., Photonics Technologies Division, Corning, NY 14831, USA.

‡ To whom all correspondence should be addressed. Tel.: +1-617-495-3760; fax: +1-617-495-9837.

E-mail address: spaepen@das.harvard.edu (F. Spaepen).

PII: S1359-6454(00)00128-2

the substrate provides good geometrical definition of the film, and in many applications film properties have to be known under just such conditions. Measurements on free-standing thin films, although geometrically more difficult, come closer to intrinsic properties of the film material and are easier to interpret.

The elastic and inelastic properties of free-standing thin films can be measured by dynamic methods [16, 17]. To know the quasistatic stiffness or to achieve the large strains required for yield or fracture, other methods are necessary, such as the tensile test [7, 18–20, 24], the bulge test [21–23] or the "drum-head" test [6]. The main difficulty with these is a reliable measurement of the strain. For the tensile test, it is essential that this measurement be made *in situ*, i.e. on the specimen itself, as one uses a strain gauge in a conventional tensile test on a bulk specimen. Without an *in situ* measurement, gripping problems and tester compliance make the strain values unreliable. A number of *in situ* methods have been developed, such as speckle interferometry [7], the interferometric strain/displacement gauge [24], or X-ray diffraction [19]. We have used an improved version [25, 26] of the laser diffraction method developed by Ruud *et al.* [20], as described below.

2. EXPERIMENTAL PROCEDURE

Layers of 99.99% pure Ag and Cu of equal thickness were deposited on glass substrates by electron-beam evaporation. The base pressure of the chamber was 2×10^{-7} torr and the deposition pressure 3×10^{-6} torr. A mask was used to produce dog-bone-shaped samples with a surface area of 2.12 cm^2, a gauge width of 3.09 mm, and a gauge length of 10 mm. Most samples had a total thickness about 3 μm, but their bilayer repeat lengths varied from 3 nm to 3 μm, depending on the number of bilayers. Pure Al (99.999%), Ag (99.99%) and Cu (99.99%) samples were deposited under similar conditions. The sample thickness was determined from the weight assuming bulk density. The results agreed with those from direct profilometer measurements to within 1%. X-ray θ–2θ diffraction [26] showed that all the thin films and multilayers were highly ⟨111⟩ textured. The grain size of the pure films was on the order of the thickness [27]. The grain size in the multilayers was on the order of the individual layer thickness [28]; this is the result of renucleation of each layer when the deposition of Ag and Cu is switched [29].

A two-dimensional photoresist grid was deposited on the film by microlithography. The unstrained pattern is a square array of photoresist islands with a 0.6 μm thickness and with a 10 μm spacing. Because the layer has a much lower modulus and forms unconnected islands, its effect on the force measurement is small. Varying the thickness of the photoresist layers of different thicknesses gave no difference in the measured results [19]. The films were peeled off their substrate for tensile testing in the apparatus shown in Fig. 1.

The sample is mounted in the copper grips on two slides. The force on the film is transmitted by a free-moving slide (♯1) and is measured by a load cell (Entran Sensors, ELF-TC-1000-2, 2 lb range) to its left. The load cell was calibrated with standard weights.† Slide ♯2 is attached to a computer-controlled, motor-driven micrometer. The film is loaded and unloaded by moving slide ♯2. A focused He–Ne laser beam (632.8 nm) is directed onto the film surface and is diffracted by the photoresist grating. Two two-dimensional diffused silicon position sensors (United Detector Technology SC20D) monitor the relative displacement of two diffracted spots. They are the third order spots in the x- and y-directions, labeled $(0, n)$ and $(n, 0)$ in Fig. 1. Ideally, when the tensile sample is strained, spot $(0, n)$ only moves in the y-direction and spot $(n, 0)$ only in the x-direction. The in-plane longitudinal and transverse strains of the film are proportional to the displacement of the laser spots in the corresponding directions.

Since the samples are free-standing, they show some wrinkling, which causes the diffraction pattern as a whole to shift. Direct effects of wrinkling on the strain measurements are eliminated by subtracting the corresponding x- and y-coordinates of the two spots. This gives reproducible data for Young's modulus if the shift of the pattern as a whole is no larger than the relative displacement of the two monitored spots. The determination of Poisson's ratio remains less reliable due to more pronounced wrinkling in the transverse direction. The tensile tes-

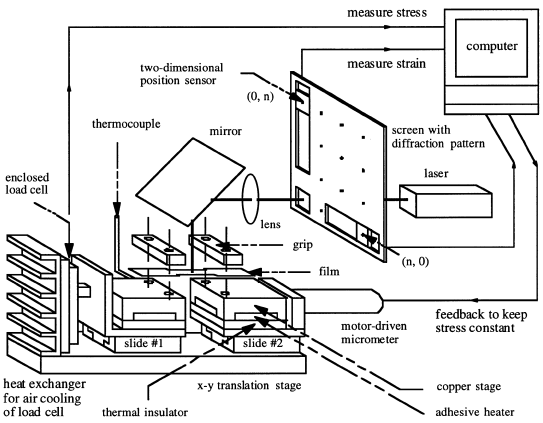

Fig. 1. A schematic diagram of the micro-tensile tester.

† The values of some of the Young's moduli reported here are slightly different from those in an earlier report [25], which were calculated based on the factory default value of the load cell sensitivity.

ter has a resolution of 0.1 MPa for the stress and 0.002% for the strain on the present samples. As shown in Fig. 1, a heating stage and a stress feedback loop have been added for tensile testing at elevated temperatures up to 120°C and creep testing at constant load. These capabilities were not used in the current study.

The data from a typical tensile test is shown in Fig. 2. Since it is impossible to mount a free-standing sample perfectly tautly, the initial stage of the test does not yield meaningful data. To straighten the film out it is necessary to apply a certain minimum load; the corresponding stress often exceeds the yield point. The laser spot is then moved over the sample to find the best, most stable diffraction pattern. At higher stress, the y position of the lower diffraction spot (n, 0) hardly shifts, indicating that the films are perfectly flat in the longitudinal direction. At several points upon further deformation into the plastic regime (up fracture) the strain rate is briefly reversed. At any point in the test, the stress is accurately known from the measurement of the load and knowledge of the cross-section (including thinning due to volume conservation during plastic deformation). Young's modulus is determined from the slopes of the unloading curves. This value is used to reconstruct the elastic part of the stress–strain curve, down to zero stress. Knowledge of the origin of the strain allows determination of the 0.2% yield stress, as shown in Fig. 2. The full stress–strain curve is the outer envelope of the data. All tests were performed at room temperature and at a strain rate of 1.1×10^{-5} s^{-1}.

This technique, like others with *in situ* strain measurement [7, 19, 24], has several advantages. First, the strain measurement occurs *in situ*: it is confined to an illuminated area of 0.3 mm diameter. This eliminates the effects of slipping in the grips or of compliance of the mechanical linkage. Second, the measurement is non-contact and therefore does not affect delicate, thin samples as a strain gauge would. Third, both longitudinal and transverse strains can be measured simultaneously. Direct measurements of the Poisson ratio are rare, and we expect that further improvements of the transverse wrinkling problem will allow direct determination of Poisson's ratio. Finally, large strains can be measured, which makes it possible to measure complete stress–strain curves. The main difficulty with the method is wrinkling of the film, which can be reduced by using dogbone samples and careful alignment.

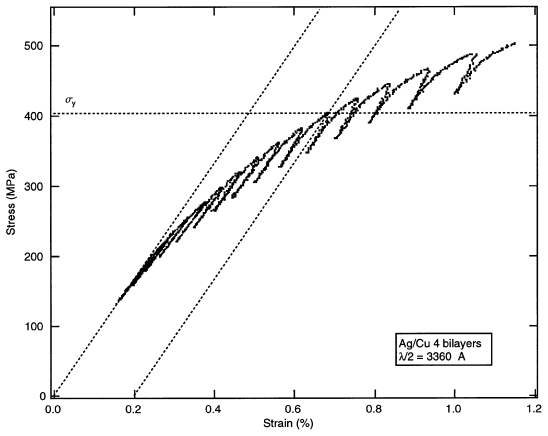

Fig. 2. Example of a stress–strain curve measured in the microtensile tester of Fig. 1. The procedures for determining Young's modulus and the yield stress σ_y are indicated.

3. RESULTS AND DISCUSSION

3.1. Young's moduli

3.1.1. Data. Figure 3(a) shows Young's modulus as a function of bilayer repeat length λ for the Ag/Cu multilayers. Data from 59 Ag/Cu samples span the range of repeat lengths between 3 nm and 3 μm. A total of 1148 loading and unloading segments are included. The Young's moduli are independent of the repeat length, and hence of grain size. Figure 3(b) summarizes the results in a histogram with bin width of 1 GPa. The distribution of the data points is clearly Gaussian. The average value is 87.5 ± 1.3 GPa, as listed in Table 1, together with the results for the pure metallic films.

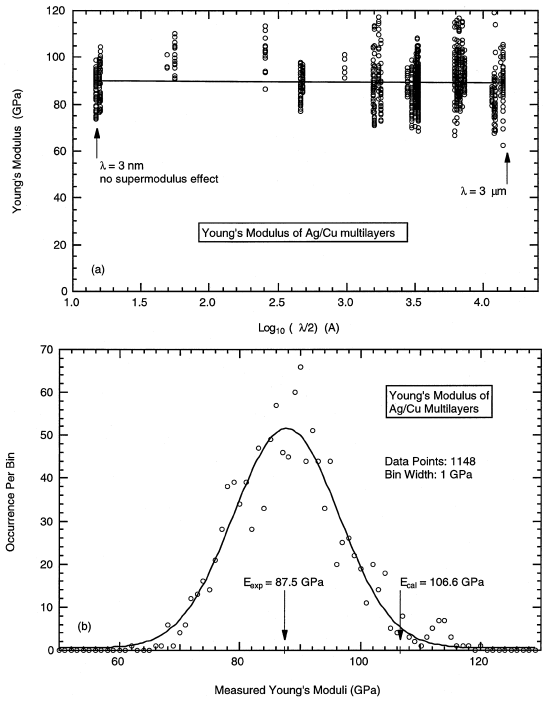

Fig. 3. Young's moduli of Ag/Cu multilayers with equal layer thicknesses. (a) The data as a function of the bilayer repeat length, λ; the nearly horizontal line is a linear fit. (b) Histogram of the data with a bin width of 1 GPa. The average measured value is 87.5 GPa; the value calculated from the literature data is 106.6 GPa.

Table 1. Summary of the Young's modulus data, with a comparison of the values calculated for a ⟨111⟩ textured film

Material	E Measured (GPa)	$E\langle 111\rangle$ Calculated (GPa)
Al	57 ± 3	71.7
Ag	63 ± 3	82.8
Cu	102 ± 7	130.3
Ag/Cu	87.5 ± 1.3	106.6

3.1.2. Discussion. Figure 3(a) shows clearly the absence of any "supermodulus" effect in these multilayers. At the 3 nm repeat length (where the effect had been reported in other systems [2, 3]) the average modulus is identical to that at other repeat lengths. This absence, in line with several earlier investigations [4, 5], indicates that the supermodulus claims were most likely the result of the difficulties in measuring elastic strain accurately in free-standing thin films.

For ⟨111⟩ textured films with cubic symmetry, the in-plane moduli are isotropic. Young's modulus can therefore be calculated exactly from tabulated bulk elastic stiffness constants [38, 39]. For the ⟨111⟩ textured Ag/Cu multilayer, Young's modulus is the average of those for ⟨111⟩ Ag and ⟨111⟩ Cu, since the layer thicknesses are equal.† All the calculated values are listed also in Table 1. In all cases the measured values are about 20% lower than the calculated ones.

Other investigators have seen a similar lowering of the stiffness in tensile tests on free-standing thin metallic films. Heinen *et al.* [6] found a lowered biaxial modulus (49 GPa, −32%) in an Al film stretched across a hole in the substrate. Read [7], using speckle interferometry for the strain measurement, found Young's moduli of 109 GPa (−16%) and 99 GPa (−24%) for electron-beam deposited Cu films and 109 GPa (−16%) for a sputtered Cu film. Interestingly, for epitaxial Si (single crystal), he found a Young's modulus equal to that of the bulk crystal.

Note that the distribution of measured moduli in Fig. 3(b) lies statistically *entirely below or at* the bulk value. This indicates that the cause of the discrepancy is the presence, to a greater or lesser degree, of microstructural features that can only *lower* the stiffness. We consider now some specific possibilities.

3.1.2.1. Texture. Ag and Cu are elastically fairly anisotropic. Young's modulus for the ⟨100⟩ texture is almost 30% lower than that for the ⟨111⟩ texture. The fraction of ⟨100⟩ grains required to give a 20% lowering of the modulus, however, is much greater than that observed in X-ray diffraction. Furthermore, in Al, which is close to elastically isotropic (6% anisotropy), the same modulus reduction is observed as in Cu, Ag or the multilayers.

3.1.2.2. Voids. It is intuitively obvious that voids lower the stiffness of a material, and a number of detailed analyses of the problem exist [30–32]. For example, to cause a 20% reduction in the Young's modulus of Al takes a volume fraction of 12% spherical voids (see Appendix A). Such a large fraction would have been visible in electron microscopy. The films also had bulk density (measured to 1% by profilometry); a 12% density deficit would have been easily detected.

3.1.2.3. Dislocation microplasticity. Reversible bowing of dislocation segments produces additional strain, and hence decreased stiffness. Friedel [33] has calculated decreases in shear modulus between 5 and 16%, depending on the nature of the dislocation network, the dislocation mobility and the slip geometry. The increase in dislocation density as a result of plastic deformation should affect these factors strongly. In our experiments, however, the order of the loading/unloading cycles along the stress–strain curve does not systematically affect the modulus.

3.1.2.4. Reversible microplasticity. The motion of dislocations that cause yielding of isolated grains can be reversible (backflow). Gibeling and Nix [34] showed that the corresponding strains can be as large as the elastic strain. This mechanism, however, is greatly diminished by glide on multiple slip systems, especially at large plastic strains. If it were the dominant cause of the modulus reduction, higher moduli should be measured in the loading/unloading cycles at large strain. This is not the case in our experiments.

3.1.2.5. More compliant grain boundaries. The imperfect packing (density deficit) in grain boundaries makes them more compliant than the bulk crystals. Grain boundaries between the smallest grains have been claimed to be particularly wide and compliant [35, 36]. It is easy to show, however, that for any reasonable assumptions about modulus averaging, boundary compliance and boundary widths, only grains smaller than 10 nm could produce modulus reductions on the order of 20% (see Appendix A). Most importantly, this mechanism implies a strong dependence of the modulus reduction on the grain size. No such dependence is observed [see Fig. 3(a)].

3.1.2.6. Microcracking. Opening of cracks is a very efficient mechanism for increasing elastic compliance [37, 38]. A likely source of microcracking is the imperfection of grain boundaries. The boundaries between the columnar grains, vertical to the film surface, are far from perfect, since adjoining

† There is a slight correction due to a difference in Poisson ratio for the two materials; the exact expression can be found in Ref. [25].

crystals are constrained by the substrate and relaxation of the boundary structure by diffusion (surface and boundary) during vapor deposition is not complete. Such microcracks are ideally oriented to increase the film compliance. It is shown in Appendix A that a 20% modulus reduction is achieved if one in three grain boundaries is fully defective or if all of them are about half defective. These values appear plausible based on the mechanism of deposition and the resulting microstructure. Importantly, this mechanism can account for the independence of the stiffness deficit on grain size, as found in this work [Fig. 3(a)], by having the flaw size scale with the dimensions of the grain boundary. The density deficit associated with microcracks is much smaller than that associated with an elastically equivalent number of voids, consistent with the dimensional measurements on the films. Even though the measurement of the Poisson ratio still needs to be improved, it is still significant that average values measured are also consistently lower than the calculated ones, as predicted by the theories on the elastic effects of microcracking [37, 38].

3.2. Yield and ductility

3.2.1. Data. Figure 4 shows a series of stress–strain curves on identical scales. They exemplify the large number of tests carried out on similar specimens. Figures 4(a) and 4(b) show that both Ag and Cu films are very ductile with ultimate tensile strengths (UTS) between 350 and 400 MPa and with plastic strains at fracture between 0.6 and 1.3%. Figures 4(c)–4(j) show a series of Ag/Cu multilayers with a total thickness around 3 mm, but with an increasing number of bilayers, corresponding to progressively smaller repeat lengths, λ. The yield stress clearly increases with decreasing λ. As shown in Figs 4(g) and 4(h), the UTS increases to a maximum between 650 and 700 MPa, and concurrently the plastic strain at fracture falls to 0.16%. In a few samples, with a small number of layers, plastic strains as large as 2.3% have been measured. For $\lambda < 80$ nm, fracture forestalls general yield, and the samples are macroscopically brittle; the UTS drops to 550–650 MPa [Figs 4(i) and 4(j)].

The functional dependence of the yield stress on the grain size is tested in different ways. Figure 5 shows the yield stress as a function of layer thickness (i.e. $\lambda/2$), which is taken as the grain size, d. A fit to a general single power law

$$\sigma_y = \sigma_0 + kd^n \tag{1}$$

gives $\sigma_0 = 109 \pm 137$ MPa, $k = 4636 \pm 3480$ MPa $(\text{Å})^{-n}$ and $n = -0.338 \pm 0.152$. The exponent is less than the classical Hall–Petch value of -0.5, although, as shown by the error estimate, barely significantly. A fit to the data using the Hall–Petch relation, i.e. equation (1) with $n = -0.5$, gives $\sigma_0 = 223 \pm 16$ MPa and $k = 0.104 \pm 0.008$ MPa $\sqrt{m}$.

Figure 6 is a classical Hall–Petch plot of the yield stress vs the inverse square root of the grain size. A straight line fit to all the data gives the same parameters as the non-linear fit for $n = -0.5$ in Fig. 6. There is hardly any evidence of decreased hardening: only the yield stress of the sample with the

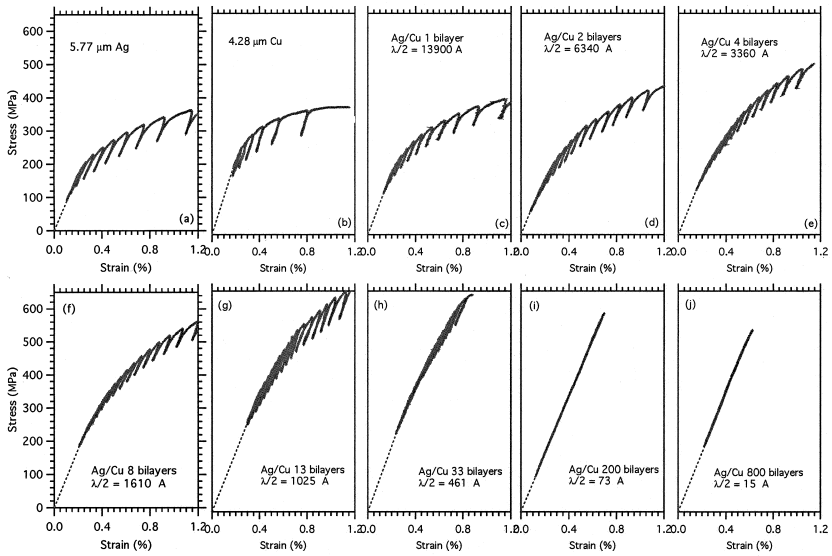

Fig. 4. Stress–strain curves with identical scales: 0–650 MPa for the stress and 0–1.2% for the strain. All tests were performed at room temperature and at a strain rate of 1.1×10^{-5} s^{-1} (a) Ag film, 5.8 μm; (b) Cu film, 4.3 μm; (c) Ag/Cu multilayer, one bilayer, $\lambda = 27{,}800$ Å; (d) Ag/Cu multilayer, two bilayers, $\lambda = 12{,}680$ Å; (e) Ag/Cu multilayer, four bilayers, $\lambda = 6720$ Å; (f) Ag/Cu multilayer, eight bilayers, $\lambda = 3220$ Å; (g) Ag/Cu multilayer, 13 bilayers, $\lambda = 2050$ Å; (h) Ag/Cu multilayer, 33 bilayers, $\lambda = 922$ Å; (i) Ag/Cu multilayer, 200 bilayers, $\lambda = 146$ Å; (j) Ag/Cu multilayer, 800 bilayers, $\lambda = 30$ Å.

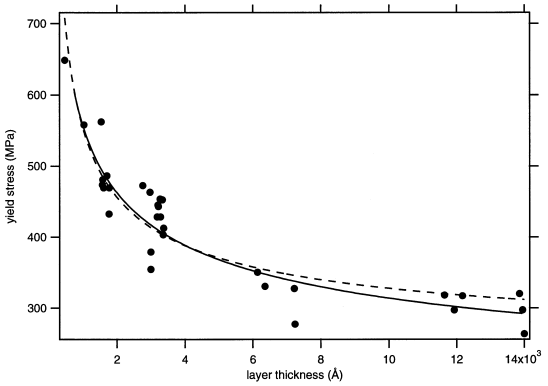

Fig. 5. Yield stress of Ag/Cu multilayers as a function of layer thickness. The solid line is a fit to the data according to a general single power law (giving $n = -0.338$); the dashed line is a fit according to the Hall–Petch relation (n set at -0.5).

smallest grain size appears slightly lower than the trend at larger grain size. A fit through all data points except the last one gives $\sigma_0 = 199 \pm 18$ MPa and $k = 0.120 \pm 0.010$ MPa $\sqrt{m}$; these parameters are not significantly different from those from the full fit.

Figure 7 shows a log–log plot of $(\sigma_y - \sigma_0)$ vs d [1], which allows comparison of our yield data to two sets of microhardness data [13] taken on samples with very different grain size. Using the Tabor relation [39] between Vickers hardness and yield stress, $\sigma_y = H_v/3$, a value of 168 MPa, derived from a Hall–Petch plot of the microhardness data on coarse-grained copper, was assigned to σ_0. Our data has an exponent $n = -0.43 \pm 0.03$, close to the value found from the general single power law fit in Fig. 5, and lies close to the extrapolation of those for the coarse-grained material.

It appears, therefore, that the classical Hall–Petch behavior observed at larger grain sizes continues to hold for the yield of these multilayers. The value of $\sigma_0 = 223$ MPa in our experiments (Fig. 6) is similar to the 168 MPa measured in the microhardness measurements on pure Cu polycrystalline samples [13], but much lower than the 600–800 MPa measured by nanoindentation on other Cu-containing multilayers [14]. The lower values are also closer to those measured in tensile tests on bulk copper [40]. The reason for the discrepancy is unclear. One possibility is the applicability of the Tabor relation between hardness and yield stress to the nanoindentation results.

Our value of the Hall–Petch slope, $k = 0.104$ MPa $\sqrt{m}$, is close to the average value of 0.15 MPa $\sqrt{m}$ found in tensile testing of bulk Cu [10] and the 0.16 MPA $\sqrt{m}$ found in nanoindentation of Cu/Nb multilayers [14]. A theoretical value for k can be calculated [41] from

$$k = 0.18\mu\sqrt{b} \tag{2}$$

where μ is the average shear modulus and b is the Burgers vector. For composites, the shear modulus of the stiffer phase is used. For copper, this gives $k = 0.138$ MPa $\sqrt{m}$. Copper is stiffer than silver (these experiments) and has about the same shear modulus as Nb (nanoindentation experiments).

As shown in Fig. 7, our data so far is consistent with the transition to softening occurring around a grain size of 30 nm, as postulated by Arzt [1] based on the data by Chokshi *et al.* [13]. Masra *et al.* [14], using nanoindentation of Cu-containing multilayers, observed decreased hardening below 50 nm and actual softening below 5 nm. Gertsman *et al.* [42]

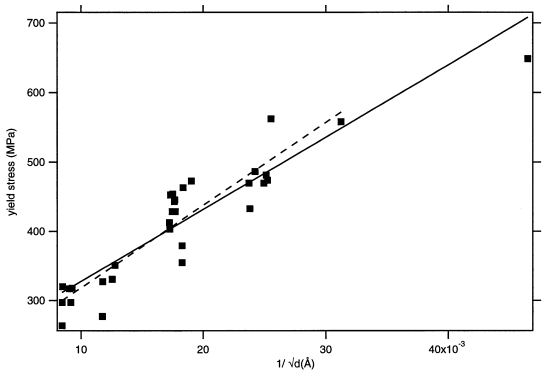

Fig. 6. Classical Hall–Petch plot of the yield stress of Ag/Cu multilayers vs the inverse square root of the layer thickness. The solid line is a straight-line fit through all the data, which gives the same fitting parameters as the non-linear fit for $n = 0.5$ in Fig. 5: $\sigma_0 = 223 \pm 16$ MPa and $k = 0.104 \pm 0.008$ MPa $\sqrt{m}$. The dashed line is a straight-line fit through all the data except the last point; it gives $\sigma_0 = 199 \pm 18$ MPa and $k = 0.120 \pm 0.010$ MPa $\sqrt{m}$.

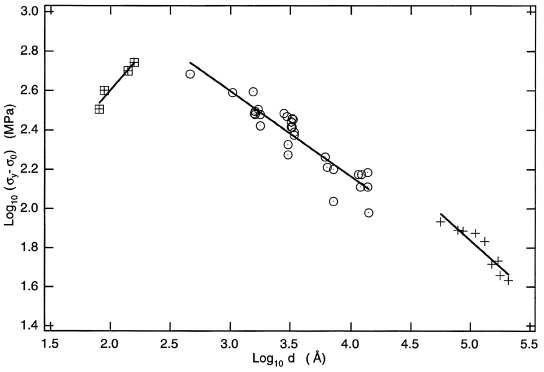

Fig. 7. Comparison of yield stresses as a function of grain size, d, from different experiments. Hardness data were converted to yield stresses by the Tabor relation, $\sigma_y = H_V/3$. Crosses: hardness data on annealed OHFC copper [from ref. 13]. Circles: yield stresses of Ag/Cu multilayers; this work. Boxed crosses: hardness data on compacted nanocrystalline copper [13]. The bulk yield stress, δ_0, is 168 MPa, as determined from a Hall–Petch plot of the hardness data on the annealed copper. The slope of the fits through the data set are: $n = -0.55 \pm 0.08$ for the annealed copper; $n = -0.43 \pm 0.03$ for the multilayers; and $n = 0.97 \pm 0.14$ for the nanocrystalline copper.

performed hardness measurements in bulk copper samples with grain sizes between 30 nm and 180 μm, and found decreased hardening below 1 μm.

Two models qualitatively explain the decreased hardening and eventual softening. Embury and Hirth appeal to a transition to a single-dislocation mechanism, based on Orowan-type bowing in the individual layers [11]. Scattergood and Koch [12] invoke the decrease in the line tension of the dislocations when the grains are small, which makes dislocation bowing easier. Arzt [1] has combined their expressions for the two regimes to give, in slightly adapted form

$$\sigma - \sigma_0 \propto \mu \left(\frac{b}{d}\right)^{0.5} \ln \frac{d}{\beta r_0} \tag{3}$$

where d/β and r_0 are, respectively, the upper and lower cutoffs of the integration of the strain energy in the calculation of the line tension of a dislocation. For $d \gg \beta r_0$, equation (3) approaches the classical Hall–Petch behavior; for d approaching βr_0, softening is predicted. The slope of a log–log plot of equation (3) gives the Hall–Petch exponent

$$n = -\frac{1}{2} + \frac{1}{\ln \frac{d}{\beta r_0}} \tag{4}$$

The maximum of equation (3) is found at $d/\beta r_0 = e^2$. On Fig. 7, the maximum hardening is seen at $d_c = 30$ nm, which gives $\beta r_0 = 4$ nm. Scattergood and Koch [12] determined $\beta r_0 = 7.7$ nm in their somewhat different analysis of the hardness data. For the grains in our experiment (d = 100 nm–1 μm) the values of the exponent obtained from equation (4) are $n = -0.18$ to $n = -0.32$, considerably smaller than the experimental value $n = -0.4$.

Although equation (3) appears to be qualitatively useful, its details still need work. The interpretation of the value of βr_0 needs attention: the assignment of r_0 must take into account the non-linear part of the elastic analysis and the value of β must reflect an analysis of the elastic screening provided by the grain boundaries. The transition between the two regimes also needs to be less gradual than the theory currently predicts.

Finally, it should be kept in mind that we have not seen any evidence for softening at the lower grain sizes. Our multilayers with the smallest repeat lengths (down to 3 nm) should provide further information on this point. Since for these repeat lengths the films remained elastic up to a fracture stress of 650 MPa, no value for their yield stress could be obtained. Since the fracture stresses are somewhat smaller than the largest yield stresses we measured, these samples may still exhibit softening. We are currently exploring this with nanoindentation.

4. CONCLUSIONS

This work has shown that our method for tensile testing, using strain measurement by optical diffraction, can be used to obtain extensive, reliable data on Young's modulus and large-strain behavior of thin films.

No variation of the stiffness with repeat length was observed, including at the smallest repeat lengths where earlier claims of a "supermodulus effect" have been made.

The stiffness of both pure films and multilayers was on average 20% lower than that calculated from literature values. Most likely, this increased compliance is the result of the presence of microcracks in the grain boundaries between the columnar grains of the vapor-deposited grains.

The variation of the yield stress with grain size follows the Hall–Petch behavior observed in other experiments at larger grain sizes. No evidence for softening at the smallest grain sizes was found. Our data can be interpolated between hardness data that show softening. The theoretical models for softening are qualitatively useful, but require quantitative refinement and further elaboration of some of the concepts they introduce.

The multilayers become increasingly stronger (UTS) and less ductile with decreasing repeat length. At the smallest wavelengths, the yield stress is too high to prevent brittle fracture.

Acknowledgements—We thank Marc Verdier, John Hirth and Subra Suresh for useful discussions, and Denis Yu for his assistance with some of the analysis and the figures. This work was supported by the Harvard Materials Research Science and Engineering Center under contract DMR 94-00396. HH acknowledges support from an AlliedSignal predoctoral fellowship.

REFERENCES

1. Arzt, E., *Acta mater.*, 1998, **46**, 5611.
2. Yang, W. M. C., Tsakalakos, T. and Hilliard, J. E., *J. Appl. Phys.*, 1977, **48**, 876.
3. Baral, D., Ketterson, J. B. and Hilliard, J. E., *J. Appl. Phys.*, 1985, **57**, 1076.
4. Davis, B. M., Seidman, A., Moreau, A., Ketterson, J. B., Mattson, J. and Grimsditch, M., *Phys. Rev. B*, 1991, **43**, 9304.
5. Cammarata, R. C., Schlesinger, T. E., Kim, C., Qadri, S. B. and Edelstein, A. S., *Appl. Phys. Lett.*, 1990, **56**, 1862.
6. Heinen, D., Bohn, H. G. and Schilling, W., *J. Appl. Phys.*, 1995, **77**, 3742.
7. Read, D. T., *Meas. Sci. Technol.*, 1998, **9**, 676.
8. Hall, E. O., *Proc. Phys. Soc. London*, 1951, **B64**, 747.
9. Petch, N. J., *J. Iron Steel Inst.*, 1953, **174**, 25.
10. Armstrong, R., Codd, I. and Douthwaite, R. M., *Phil. Mag.*, 1962, **7**, 45.
11. Embury, J. D. and Hirth, J. P., *Acta metall. mater.*, 1994, **42**, 2051.
12. Scattergood, R. O. and Koch, C. C., *Scripta metall. mater.*, 1992, **27**, 1195.
13. Chokshi, A. H., Rosen, A., Karch, J. and Gleiter, H., *Scripta metall.*, 1989, **23**, 1679.
14. Misra, A., Verdier, M., Lu, Y. C., Kung, H.,

Mitchell, T. E., Nastasi, M. and Embury, J. D., *Scripta mater*., 1998, **39**, 555.
15. Nix, W. D., *Metall. Trans. A*, 1989, **20A**, 2217.
16. Bobbin, S. E., Wagner, J. W. and Cammarata, R. C., *Appl. Phys Lett*., 1991, **59**, 1544.
17. Moreau, A., Ketterson, J. B. and Huang, J., *Mater. Sci. Eng. A*, 1990, **126**, 149.
18. Baral, D., Ketterson, J. B. and Hilliard, J. E., *J. Appl. Phys*., 1985, **57**, 1076.
19. Kretschmann, A., Kuschke, W. M., Baker, S. P. and Arzt, E., *Mater. Res. Symp. Proc*., 1997, **436**, 59.
20. Ruud, J. A., Josell, D., Spaepen, F. and Greer, A. L., *J. Mater. Res*., 1993, **8**, 112.
21. Tsakalakos, T. and Hilliard, J. E., *J. Appl. Phys*., 1983, **54**, 734.
22. Small, M. K., Daniels, B. J., Clemens, B. M. and Nix, W. D., *J. Mater. Res*., 1994, **9**, 25.
23. Vlassak, J. J. and Nix, W. D., *J. Mater. Res*., 1992, **7**, 3242.
24. Sharpe Jr, W. N., *Opt. Engng*, 1982, **21**, 483.
25. Huang, H. and Spaepen, F., *Mater. Res. Soc. Symp. Proc*., 1996, **405**, 501.
26. Huang, H., Ph.D. thesis, Harvard University, 1998.
27. Thompson, C. V. and Carel, R., *J. Mech. Phys. Solids*, 1996, **44**, 657.
28. Verdier, M., private communication.
29. Shull, A. and Spaepen, F., *J. Appl. Phys*., 1996, **80**, 6243.
30. Mackenzie, J. K., *Proc. Phys. Soc. B*, 1950, **63**, 2.
31. Eshelby, J. D., *Proc. Roy. Soc. London A*, 1957, **241**, 376.
32. Budiansky, B., *J. Mech. Phys. Sol*., 1965, **13**, 223.
33. Friedel, J., in *Dislocations*. Pergamon, Oxford, 1964, p. 243.
34. Gibeling, J. C. and Nix, W. D., *Acta metall*., 1981, **29**, 1769.
35. Korn, D., Morsch, A., Birringer, R., Arnold, W. and Gleiter, H., *J. Phys*., 1988, **C5**, 769.
36. Weller, M., Diehl, J. and Schaefer, H. E., *Phil. Mag*., 1991, **A63**, 527.
37. Budiansky, B. and O'Connell, R. J., *Int. J. Solids Structures*, 1976, **12**, 81.
38. Laws, N. and Brockenbrough, J. R., *Int. J. Solids Structures*, 1987, **23**, 1247.
39. Tabor, D., *The Hardness of Metals*. Clarendon Press, Oxford, 1951.
40. Frost, H. J. and Ashby, M. F., in *Deformation Mechanism Maps*. Pergamon, Oxford, 1982, p. 24.
41. Gil Sevillano, J., Plastic deformation and fracture of materials, in *Materials Science and Technology—A Comprehensive Treatment*, Vol. 6, ed. H. Mughrabi. VCH, New York, 1993.
42. Gertsman, V. Y., Hoffmann, M., Gleiter, H. and Birringer, R., *Acta metall. mater*., 1994, **42**, 3539.
43. Fu, Y. and Evans, A. G., *Acta metall*., 1985, **33**, 1515.

APPENDIX A

Calculations of enhanced compliance of thin films with columnar microstructure

The columnar microstructure of a film or an individual layer in a multilayer is illustrated in Fig. A1. Three mechanisms for compliance enhancement are illustrated. The grains are hexagonal prisms, with height and diameter both equal to d. Their edge length is $d/2$ and their volume is $V_g = (3\sqrt{3})/8\ d^3 = 0.65\ d^3$.

Voids

Following Eshelby [31], the effective bulk modulus, K_{eff}, and shear modulus, μ_{eff}, of an isotropic material with bulk modulus K and shear modulus μ containing a volume fraction of randomly distributed, non-interacting, spherical voids f, are

$$K_{\text{eff}} = \frac{K}{1 + Af} \tag{A1}$$

and

$$\mu_{\text{eff}} = \frac{\mu}{1 + Bf} \tag{A2}$$

where

$$A = 1 + \frac{3K}{4\mu} \tag{A3}$$

and

$$B = \frac{5(3K + 4\mu)}{9K + 8\mu} \tag{A4}$$

The effective Young's modulus is then

$$E_{\text{eff}} = \frac{9K_{\text{eff}}}{1 + \dfrac{3K_{\text{eff}}}{\mu_{\text{eff}}}} \tag{A5}$$

Using K = 76 GPa and $\mu = 20$ GPa (for Al, which is close to isotropic), one finds by numeric solution that the experimentally observed $E_{\text{eff}}/E = 0.8$ corresponds to $f = 0.12$.

Grain boundary compliance

In this mechanism, the grain boundaries have a thickness δ and a Young's modulus E', as illustrated by grain B in Fig. A1. A simple, approximate calculation of the effective modulus is illustrated by Fig. A2. It consists of two steps: (i) calculating the effective modulus of region I, which contains grain boundaries parallel to the direction of the stress and (ii) calculating the effective modulus of this

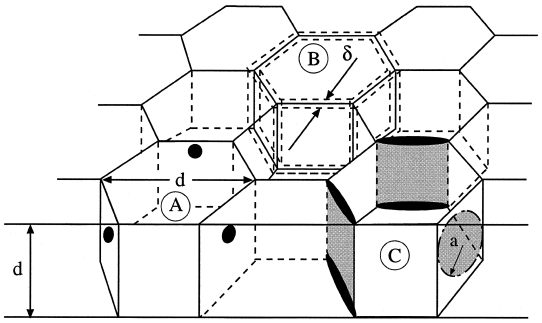

Fig. A1. Schematic diagram of flaws in a thin film with a columnar diagram that enhance compliance. A: voids; B: grain boundaries; C: microcracks at the grain boundaries.

region in series with region II, which is a continuous grain boundary region perpendicular, on the average, to the stress.

Region I contains one grain boundary of width δ, and has a repeat length of $d\sqrt{3}/2$. The effective modulus for this parallel region is then

$$E^*_{\text{eff}} = \frac{\delta E + (d\sqrt{3}/2 - \delta)E}{d\sqrt{3}/2} \tag{A6}$$

Region II contains a wavy grain boundary, which is approximated by a straight one of equal volume, and hence of thickness $2\delta/\sqrt{3}$. Its repeat distance is 3 d/4. Regions I and II are loaded in series and their effective modulus, E_{eff}, is then given by

$$\frac{3d/4}{E_{\text{eff}}} = \frac{3d/4 - 2\delta/\sqrt{3}}{E^*_{\text{eff}}} + \frac{2\delta/\sqrt{3}}{E'} \tag{A7}$$

Numerical solutions of these equations are easily obtained. For example, taking $E'/E = 0.5$, which corresponds to a very compliant boundary, the experimentally observed 20% reduction in effective modulus is obtained for $\delta/d = 0.12$, which corresponds to a very small grain size.

Microcracking

The effect on the compliance of slit-type microcracks of width a, randomly distributed among the grain boundaries of a hexagonal columnar array of grains (see grain C in Fig. A1), was first calculated by Fu and Evans [43]. Laws and Brockenbrough [38] later showed that Evans–Fu result was exactly equivalent to that for two-dimensionally randomly distributed slit-type cracks. At small concentrations of cracks, they derived the following expression for the effective modulus

$$\frac{E_{\text{eff}}}{E} = 1 - \frac{\pi^2}{4}(1 - \nu^2)\varepsilon \tag{A8}$$

where ν is Poisson's ratio and ε is an effective crack density, introduced by Budiansky and O'Connell [37] and defined as

$$\varepsilon = \frac{2N}{\pi}\left\langle \frac{A^2}{P} \right\rangle \tag{A9}$$

where N is the number of cracks per unit volume, A is the crack area, and P is the crack perimeter. For slits of width a and height d:

$$\varepsilon = \frac{2N}{\pi}\,\frac{a^2 d^2}{2(a+d)} \tag{A10}$$

For $E_{\text{eff}}/E = 0.8$, as seen in the experiments, and $\nu = 0.3$ (the results are insensitive to the choice), equation (A8) gives $\varepsilon = 0.089$. To interpret this number, we consider two cases.

First, consider a fully detached boundary, i.e. $a = d/2$. Equation (A10) then gives $N = 1.68/d^3$. The number of such boundaries per grain is then $NV_g = 1.09$, or one per grain.

Second, consider the case of all boundaries being flawed to the same extent (i.e. all have a slit of width a). Since there are three boundaries per grain, the number of cracks per unit volume becomes $N = 3/V_g = 4.61/d^3$. Inserting this value into equation (A10) and solving gives $a = 0.28\ d$. Since the boundaries are $d/2$ wide, this means that about half of their area must be detached.

This result is insensitive to the crack geometry. For example, consider each boundary containing a penny-shaped crack of radius a. For this geometry, equation (A9) reduces to:

$$\varepsilon = N\langle a^3 \rangle \tag{A11}$$

Although Laws and Brockenbrough [38] did not consider this case, they showed that the results for slits and pennies are very close for aligned cracks; Budiansky and O'Connell [37] had shown the same for three-dimensionally randomly distributed cracks. We will therefore also use equation (A8) for this case, and put $\varepsilon = 0.089$. The number of cracks per unit volume is the same as in the previous case: $N = 3/V_g = 4.61/d^3$. Equation (A11) then gives $a = 0.268\ d$. The corresponding ratio of the crack area to the boundary area is 0.45.

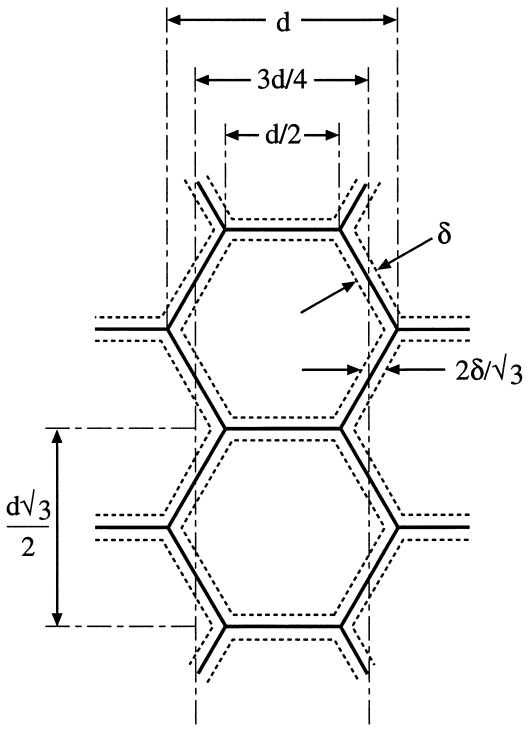

Fig. A2. Diagram illustrating the calculation of the composite compliance of columnar grains separated by a grain boundary region with a different compliance.